nature geoscience

LETTERS

PUBLISHED ONLINE: 12 OCTOBER 2015 | DOI: 10.1038/NGEO2563

Divergent trajectories of Antarctic surface melt under two twenty-first-century climate scenarios

Luke D. Trusel[1,2*], Karen E. Frey[2], Sarah B. Das[1], Kristopher B. Karnauskas[1], Peter Kuipers Munneke[3,4], Erik van Meijgaard[5] and Michiel R. van den Broeke[3]

Ice shelves modulate Antarctic contributions to sea-level rise[1] and thereby represent a critical, climate-sensitive interface between the Antarctic ice sheet and the global ocean. Following rapid atmospheric warming over the past decades[2,3], Antarctic Peninsula ice shelves have progressively retreated[4], at times catastrophically[5]. This decay supports hypotheses of thermal limits of viability for ice shelves via surface melt forcing[3,5,6]. Here we use a polar-adapted regional climate model[7] and satellite observations[8] to quantify the nonlinear relationship between surface melting and summer air temperature. Combining observations and multimodel simulations, we examine melt evolution and intensification before observed ice shelf collapse on the Antarctic Peninsula. We then assess the twenty-first-century evolution of surface melt across Antarctica under intermediate and high emissions climate scenarios. Our projections reveal a scenario-independent doubling of Antarctic-wide melt by 2050. Between 2050 and 2100, however, significant divergence in melt occurs between the two climate scenarios. Under the high emissions pathway by 2100, melt on several ice shelves approaches or surpasses intensities that have historically been associated with ice shelf collapse, at least on the northeast Antarctic Peninsula.

Antarctic ice shelves have undergone widespread and accelerated thinning and retreat in recent decades in response to coupled atmospheric and oceanic forcing[3–5,9,10]. On the Antarctic Peninsula (AP), this recession has been particularly pronounced and punctuated with near-uniform, abrupt collapses of Larsen A, Prince Gustav, and Larsen B ice shelves occurring since 1995 (Fig. 1). Across this region, recent atmospheric warming has exceeded global average rates[2] and current surface melting levels are unprecedented over the past millennium on the northeast AP (ref. 11). This warming and melt intensification has directly led to an expansion of meltwater ponding, and the resultant hydrofracturing is considered a leading mechanism of AP ice shelf collapse[3,5,12].

All Antarctic ice shelves experience surface melting today[7,8], yet ocean-induced basal melting at present dominates ice shelf mass losses, particularly outside of the AP (refs 9,10). Nevertheless, surface melt intensities approach those of the AP elsewhere in Antarctica (Fig. 1c), meltwater ponding exists beyond the AP (refs 13,14), and strong basal melting can hasten ice shelf destabilization[4,10]. The question therefore arises, are recent ice shelf dynamics on the AP indicative of forthcoming changes elsewhere in Antarctica? Understanding the present-day and future viability of all Antarctic ice shelves requires an improved characterization of the sensitivity of ice shelves to temperature change, a better historical context for AP melt acceleration and ice shelf collapse, and robust projections of future pan-Antarctic change.

Air temperature is often used to parameterize surface melt owing to several important physical linkages with the surface energy balance ultimately responsible for meltwater production[15]. Previous research on the AP has empirically demonstrated exponential relationships between positive degree-days (PDD) and mean annual[16,17] or summer[11] (December–February; DJF) air temperature. Because of established melt–PDD links and recent AP warming, PDD–temperature nonlinearity has been invoked to infer a nonlinear and relatively high sensitivity of melt on glaciers and ice shelves on the AP to fluctuations in mean temperature[11,18]. However, a direct melt–temperature relationship has yet to be established.

We improve on these previous studies by quantifying the relationship between mean DJF 2-m air temperature (T_{2m}) and surface meltwater production on ice shelves across Antarctica. We utilized multiple forcings of the regional climate–snowpack model, RACMO2 (ref. 7), and independent satellite-derived melt observations[8] to robustly quantify ice shelf surface melt responses to changing summer T_{2m} across a broad spectrum of present-day and projected conditions (see Methods). We find the melt–temperature sensitivity is well characterized by an exponential function for all Antarctic ice shelves (Fig. 1a). Physically underpinning this nonlinearity are longer melt seasons, the positive melt-albedo feedback, and increased downward longwave radiation and turbulent heat fluxes with increasing air temperatures. Indeed (as previous PDD–T_{2m} relationships[11,16,17] suggest), T_{2m} variability above warmer ice shelves experiencing already high levels of melt results in disproportionally larger impacts to meltwater production than for colder, lower-melt ice shelves.

The exponential melt–T_{2m} relationship described above provides an important contextual linkage between observed warming and melt acceleration associated with ice shelf destabilization. Observed temperatures[19] from the nearest permanent weather station to recent northeast AP ice shelf collapses, Base Marambio, reveal a 1.95 °C summer warming between 1971–1975 and 2005–2009 (the first and last pentads of the record with full DJF observations). Applying our established melt–T_{2m} relationship (Fig. 1a), this observed warming would equate to a melt increase from 351 mm w.e. (water equivalence) yr^{-1} to 852 mm w.e. yr^{-1} (~140% increase in melt). Although Marambio is not located over permanent ice, its recorded temperatures are regionally representative (Supplementary Fig. 1)

[1]Department of Geology and Geophysics, Woods Hole Oceanographic Institution, Woods Hole, Massachusetts 02543, USA. [2]Graduate School of Geography, Clark University, Worcester, Massachusetts 01610, USA. [3]Institute for Marine and Atmospheric Research, Utrecht University, 3584 CC Utrecht, Netherlands. [4]Department of Geography, Swansea University, Swansea SA2 8PP, UK. [5]Royal Netherlands Meteorological Institute, 3730 AE De Bilt, Netherlands. *e-mail: ltrusel@whoi.edu

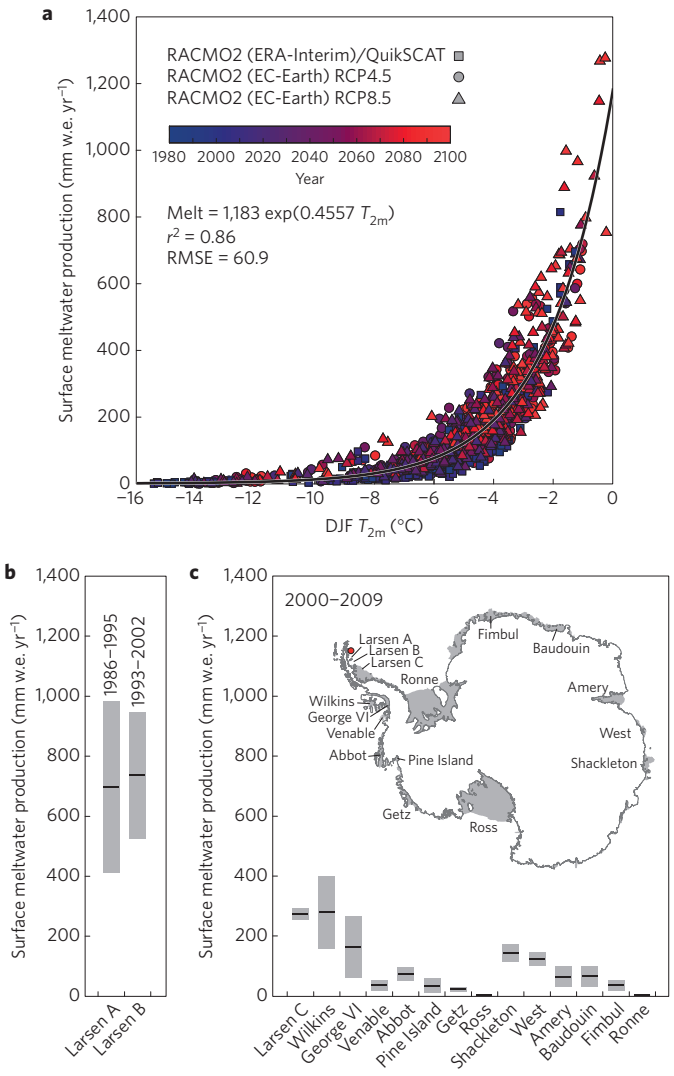

Figure 1 | Melt–temperature nonlinearity and recent melting conditions. **a**, Relationship between mean summer (DJF) 2-m air temperature (T_{2m}) and surface melt over ten-year periods from 48 Antarctic ice shelves (see Methods). **b**, Mean (horizontal black lines) and ±1 temporal standard deviation (s.d.; shaded area) of melt modelled by RACMO2 across Larsen A and B in the respective decades before their collapses. **c**, Mean melt (±1 inter-method s.d.) over 2000–2009 from two forcings of RACMO2 and satellite observations[8]. Red dot on map in **c** shows location of James Ross Island and Base Marambio.

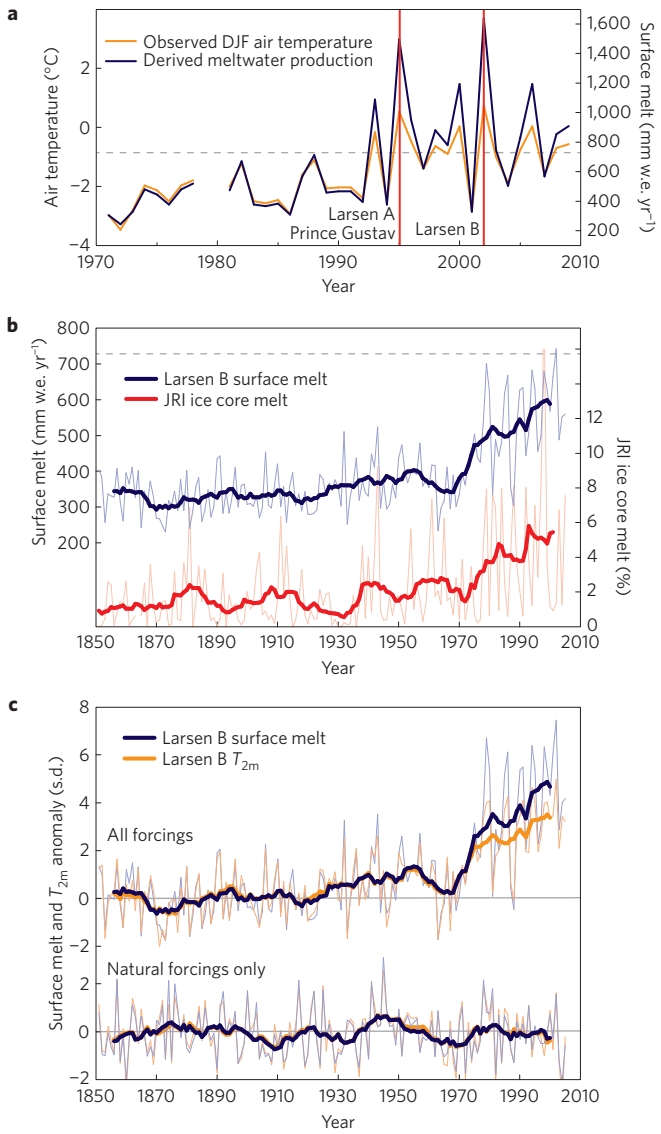

Figure 2 | Historical melt evolution before ice shelf collapse. **a**, Observed air temperatures at Marambio and derived melt levels. Vertical red lines show years of collapse for indicated ice shelves. **b**, Melt derived from GCM Ensemble simulations and an ice core record of past melt intensity from James Ross Island (JRI; melt as a percentage of annual accumulation)[11]. **c**, Anomalies (from 1851 to 1900) in melt and temperature from GCM Ensemble simulations including and excluding anthropogenic forcing. Bold lines (in **b**,**c**) show 11-year centred moving averages. Dashed horizontal lines (in **a**,**b**) show average pre-collapse melt on Larsen A and B simulated by RACMO2.

and this derived melt intensification is consistent with melt simulated by RACMO2 on the now-collapsed Larsen A and B (Fig. 1b), as well as previous ground-based assessments[20,21] of pre-collapse melt levels. Furthermore, we find melt immediately preceding collapses of Larsen A and B significantly exceeded that on surrounding ice shelves that remained intact (Supplementary Fig. 2). Our results also indicate that years of observed collapses (1995 and 2002), although only marginally warmer than surrounding years, appear to be the two years of highest meltwater production on the northeast AP since these observations commenced (Fig. 2a).

To characterize ice shelf melting more directly and within a longer temporal framework, we investigated T_{2m} simulated by a subset of five well-suited global climate models (hereafter 'GCM Ensemble') from the Coupled Model Intercomparison Project 5 (ref. 22; CMIP5; see Methods). Using the melt–T_{2m} sensitivity (Fig. 1a) and the multimodel T_{2m} from CMIP5 Historical simulations (post-1851), we find a marked increase in Larsen B melt beginning in the early 1970s. This modelled melt intensification closely corresponds with observed increases in melt from the adjacent James Ross Island ice cap[11] (Fig. 2b), thereby supporting the melt–T_{2m} sensitivity analysis and revealing that recent warming is well constrained within the GCM Ensemble. Anomalies in modelled melt and T_{2m} uniformly vary until the early 1970s warming, after which melt anomalies far exceed those in T_{2m} (Fig. 2c). Furthermore, our results indicate a recent regime shift of the northeast AP towards higher melt–T_{2m} sensitivities, whereby interannual temperature variability results in disproportionately larger variability in melt (Fig. 2 and Supplementary Figs 3 and 4).

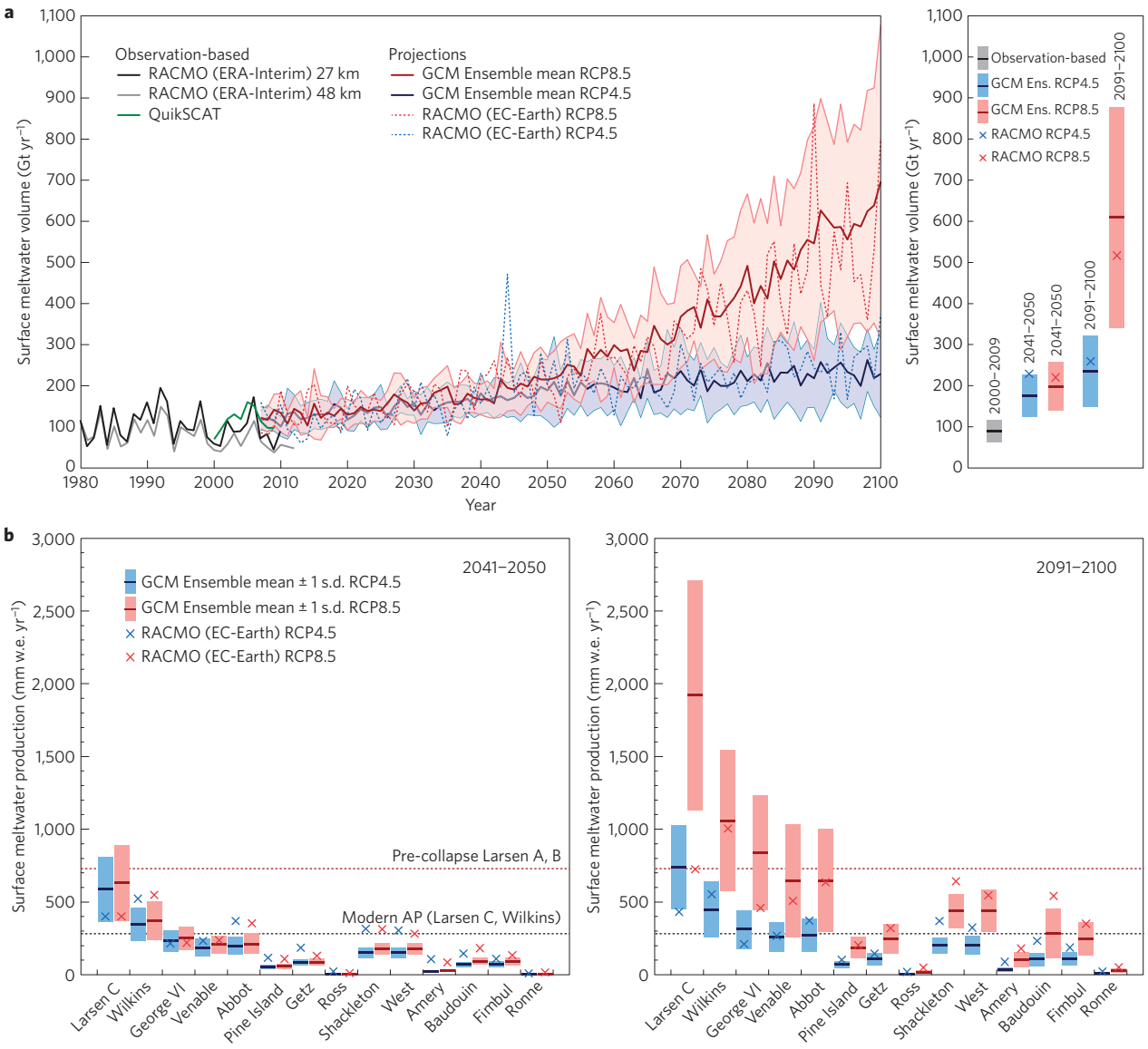

Figure 3 | Twenty-first-century evolution of Antarctic surface melt. a, Antarctic-wide volume of surface meltwater production from reanalysis-driven RACMO2 simulations and QuikSCAT satellite observations[8], as well as projected under two future climate scenarios. Right: mean Antarctic meltwater volume ± 1 s.d. (shaded) at indicated decades. **b**, Modelled meltwater production across individual ice shelves at the middle (left) and end (right) of the twenty-first century. Dotted red lines represent the mean collapse-associated melt on Larsen A and B; dotted black lines show average recent melt on Larsen C and Wilkins on the AP (from Fig. 1c).

We can assess the mechanisms responsible for the modelled warming and surface melt intensification by evaluating simulations that include and exclude transient anthropogenic forcing agents. We find the recent warming and melt intensification on Larsen B is only reproduced using GCM experiments imposing anthropogenic forcing (Fig. 2c). These results therefore support findings that the recent AP melt intensification could occur only after sufficient summer warming[11] and of important anthropogenic influence on AP warming beyond stratospheric ozone forcing of the Southern Annular Mode[11,23].

We next employed two novel melt modelling approaches (forced by GCM experiments) to assess a range of potential future melt trajectories across all Antarctica ice shelves. RACMO2 forced by the EC-Earth2.3 GCM provides robust, physically based twenty-first-century melt projections (see Methods). We also applied our melt–T_{2m} sensitivity calibration (Fig. 1a) to models in the GCM Ensemble (see Methods). We considered two distinct future emissions trajectories under which to assess the evolution of Antarctic surface melting, namely Representative Concentration Pathways RCP4.5 and RCP8.5, representing intermediate and high (~4.5 and ~8.5 W m^{-2}) energy imbalances by the end of the twenty-first century[22].

By mid-century under RCP4.5, the total annual volume of surface meltwater produced across Antarctica doubles from recent levels (88 ± 26 Gt yr^{-1}) to 177 ± 52 Gt yr^{-1}, yet undergoes relatively little increase afterwards (Fig. 3a). Under RCP8.5, the Antarctic melt volume increases similarly by 2050 (199 ± 60 Gt yr^{-1}), but then exhibits significant divergence from the RCP4.5 simulations beyond mid-century. Moreover, owing to the nonlinearity described above, by 2090–2100 the multimodel mean meltwater volume projected under RCP8.5 accelerates to 613 ± 258 Gt yr^{-1} (Fig. 3a). For perspective, this end-of-century volume of surface meltwater is nearly identical to that produced annually across Greenland over 2001–2006 (ref. 24), although the ice sheet area experiencing melt in Antarctica

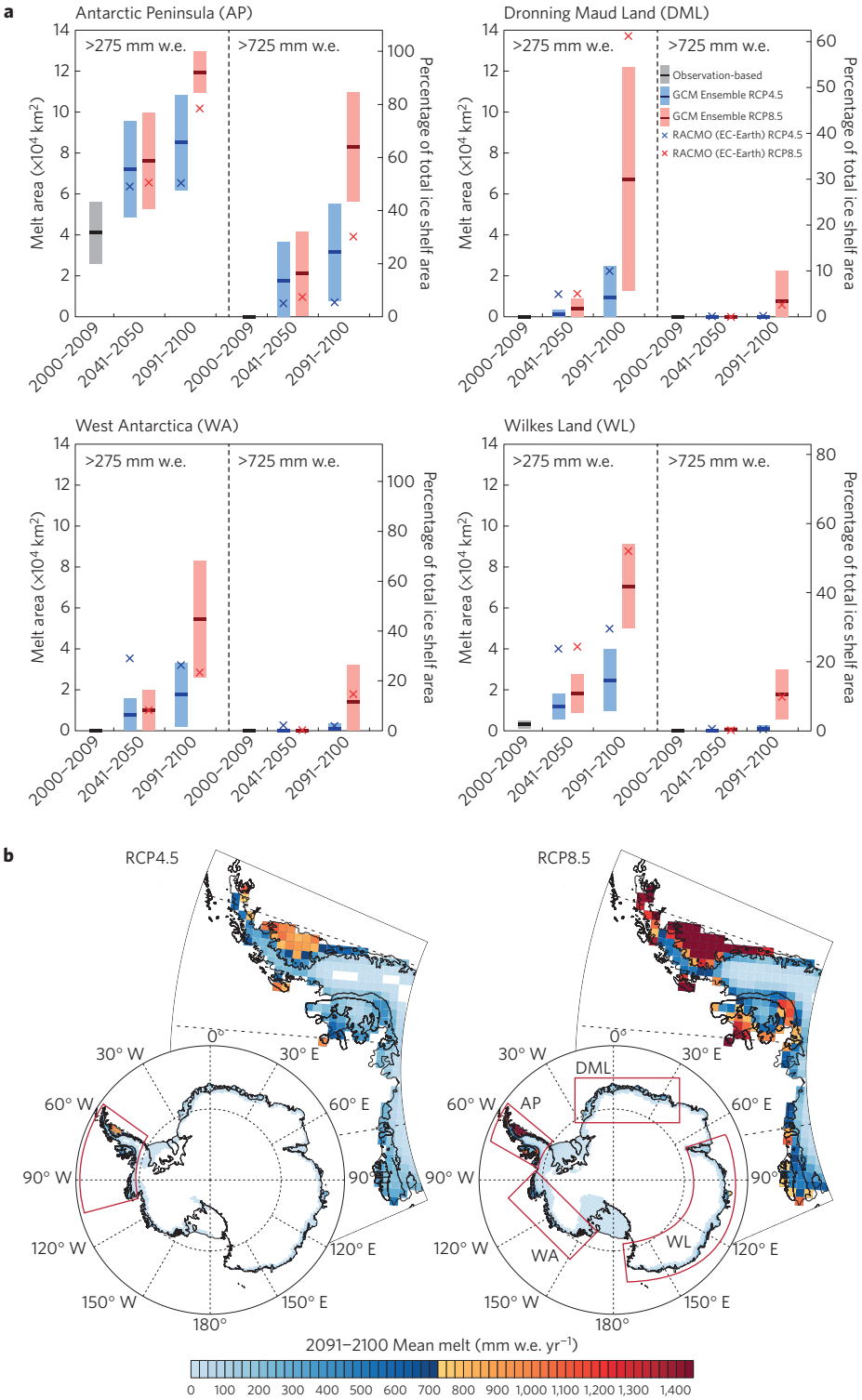

Figure 4 | Melt exceeding specific thresholds across time and space. a, Plots of regional ice shelf areas exceeding melt levels prevailing at present on high-melt AP ice shelves (>275 mm w.e. yr^{-1}) and associated with ice shelf collapses (>725 mm w.e. yr^{-1}). Regions indicated in **b**. **b**, Mean surface melting over 2091–2100 derived from the GCM Ensemble under RCP4.5 and RCP8.5. Enlarged maps show the AP and a portion of West Antarctica (map area indicated in red outline in the full RCP4.5 map). Boundary between blue and orange colours represents historical northeast AP collapse-associated melt level.

is approximately 2.5 times the recent melting area in Greenland. The strong divergence in the meltwater volume simulated between RCP4.5 and RCP8.5 after 2050 closely follows pathways of atmospheric CO_2 concentrations (Supplementary Fig. 5) and radiative forcing under these scenarios, underscoring the importance of these differing paths of sustained anthropogenic forcing on Antarctic climate evolution.

We additionally investigated simulations of scenario-dependent melt trajectories across 14 regionally representative Antarctic ice shelves (Fig. 3b). Regardless of scenario at mid-century, melt

increases to two- to threefold on average from recent levels across nearly all Antarctic ice shelves (Fig. 3b). After 2050, only marginal melt increases occur under RCP4.5. This scenario starkly contrasts with RCP8.5, under which significant and widespread melt intensification continues across many ice shelves over the full century (Fig. 3b).

To assess the significance of modelled surface melt trajectories, we first consider a threshold of 275 mm w.e. yr^{-1}, the recent average melt on Larsen C and Wilkins of the AP (Fig. 1c; the two highest melting ice shelves existing today). Across Antarctica, many ice shelves in at least one modelling method approach this present-day high-melt level by 2050 (black dotted line, Fig. 3b). This mid-century intensification occurs irrespective of RCP scenario and includes nearly 60% of the total ice shelf area on the AP (~25% areal increase from today; Fig. 4a). The total ice shelf area exceeding this melt level further increases in all regions towards 2100, particularly under RCP8.5, representing a great contrast to melt conditions prevailing at present across Antarctica (Fig. 4a). The glaciological ramifications of this Antarctic-wide surface melt intensification may be expected to be similar to that of the present-day AP. Today, AP surface melt contributes to ice shelf thinning, firn air content depletion, and meltwater ponding[8,12,25]—all important precursors for ice shelf collapse[26]. Furthermore, AP glaciers have almost uniformly thinned, retreated and accelerated in response to the recent atmospheric warming and the consequential reduction of outlet glacier and ice shelf buttressing[27,28].

Melt intensities preceding the collapses of Larsen A and B (725 mm w.e. yr^{-1}; Fig. 1b) offer an additional value with which to assess the potential severity of future melt evolution. Melt on multiple ice shelves approaches or exceeds this northeast AP collapse-associated level by 2100, particularly in RCP8.5 (Figs 3b and 4). Portions of ice shelves in all regions exceed 725 mm w.e. yr^{-1} of melt (Fig. 4a), but increases are most pronounced on the AP, where under RCP8.5 portions of nearly all AP ice shelves surpass this level by 2100 (Fig. 4b). An important distinction is that this degree of melt intensification is unique to the RCP8.5 scenario and is overwhelmingly absent under RCP4.5, particularly outside of the AP region (Fig. 4a). Many factors beyond surface melt ultimately determine ice shelf viability, including ice shelf thickness and bedrock pinning characteristics[4,5], as well as the ability of firn to accommodate melt refreeze[26]. Ice shelf breakup and retreat can also occur in the absence of strong surface melting (for example, ref. 29; Supplementary Fig. 2). Thus, although ice shelves respond heterogeneously to external forcing and our projections of high melt do not foretell ice shelf collapse, melt levels associated with RCP8.5 on many ice shelves raise concern about their future viability. This concern is heightened when considering surface melt intensification may not be impacting ice shelves in isolation, but rather in tandem with strong basal melting that similarly responds nonlinearly to ocean temperature increases[30] and is already in place across much of Antarctica today[9,10,25].

Observations and climate–snowpack modelling reveal that Antarctic ice shelf surface melting is exponentially related to summer near-surface air temperature. Recent AP summer warming has resulted in a high sensitivity of ice shelves in this region to further temperature change, culminating in high-melt conditions linked to ice shelf collapses. Twenty-first-century climate simulations indicate pan-Antarctic ice shelf melt intensification under both high and intermediate emissions scenarios, but importantly show significant divergence beyond mid-century. Notably by 2100 under the high emissions RCP8.5 scenario, multiple ice shelves reach melt levels presently characteristic of the AP, as well as approach or surpass melt intensities uniquely associated with previous collapse events. Future melt trajectories are intimately tied to current and future climate pathways, thus highlighting a critical anthropogenic control on the future evolution of the Antarctic ice sheet and its potential contributions to global sea level.

Methods

Methods and any associated references are available in the online version of the paper.

Received 12 May 2015; accepted 14 September 2015; published online 12 October 2015

References

1. Joughin, I. & Alley, R. B. Stability of the West Antarctic ice sheet in a warming world. *Nature Geosci.* **4,** 506–513 (2011).
2. Turner, J. *et al.* Antarctic climate change during the last 50 years. *Int. J. Climatol.* **25,** 279–294 (2005).
3. Vaughan, D. G. & Doake, C. S. M. Recent atmospheric warming and retreat of ice shelves on the Antarctic Peninsula. *Nature* **379,** 328–331 (1996).
4. Cook, A. J. & Vaughan, D. G. Overview of areal changes of the ice shelves on the Antarctic Peninsula over the past 50 years. *Cryosphere* **4,** 77–98 (2010).
5. Scambos, T. A., Hulbe, C., Fahnestock, M. & Bohlander, J. The link between climate warming and break-up of ice shelves in the Antarctic Peninsula. *J. Glaciol.* **46,** 516–530 (2000).
6. Mercer, J. H. West Antarctic ice sheet and CO_2 greenhouse effect: A threat of disaster. *Nature* **271,** 321–325 (1978).
7. Kuipers Munneke, P., Picard, G., van den Broeke, M. R., Lenaerts, J. T. M. & van Meijgaard, E. Insignificant change in Antarctic snowmelt volume since 1979. *Geophys. Res. Lett.* **39,** L01501 (2012).
8. Trusel, L. D., Frey, K. E., Das, S. B., Kuipers Munneke, P. & van den Broeke, M. R. Satellite-based estimates of Antarctic surface meltwater fluxes. *Geophys. Res. Lett.* **40,** 6148–6153 (2013).
9. Pritchard, H. D. *et al.* Antarctic ice-sheet loss driven by basal melting of ice shelves. *Nature* **484,** 502–505 (2012).
10. Paolo, F. S., Fricker, H. A. & Padman, L. Volume loss from Antarctic ice shelves is accelerating. *Science* **348,** 327–331 (2015).
11. Abram, N. J. *et al.* Acceleration of snow melt in an Antarctic Peninsula ice core during the twentieth century. *Nature Geosci.* **6,** 404–411 (2013).
12. Scambos, T. *et al.* Ice shelf disintegration by plate bending and hydro-fracture: Satellite observations and model results of the 2008 Wilkins ice shelf break-ups. *Earth Planet. Sci. Lett.* **280,** 51–60 (2009).
13. Miles, B. W. J., Stokes, C. R., Vieli, A. & Cox, N. J. Rapid, climate-driven changes in outlet glaciers on the Pacific coast of East Antarctica. *Nature* **500,** 563–566 (2013).
14. Kingslake, J., Ng, F. & Sole, A. Modelling channelized surface drainage of supraglacial lakes. *J. Glaciol.* **61,** 185–199 (2015).
15. Ohmura, A. Physical basis for the temperature-based melt-index method. *J. Appl. Meteorol.* **40,** 751–761 (2001).
16. Vaughan, D. G. Recent trends in melting conditions on the Antarctic Peninsula and their implications for ice-sheet mass balance and sea level. *Arct. Antarct. Alp. Res.* **38,** 147–152 (2006).
17. Barrand, N. E. *et al.* Trends in Antarctic Peninsula surface melting conditions from observations and regional climate modeling. *J. Geophys. Res.* **118,** 315–330 (2013).
18. Davies, B. J. *et al.* Modelled glacier response to centennial temperature and precipitation trends on the Antarctic Peninsula. *Nature Clim. Change* **4,** 993–998 (2014).
19. Turner, J. *et al.* The SCAR READER project: Toward a high-quality database of mean Antarctic meteorological observations. *J. Clim.* **17,** 2890–2898 (2004).
20. Sergienko, O. & Macayeal, D. R. Surface melting on Larsen ice shelf, Antarctica. *Ann. Glaciol.* **40,** 215–218 (2005).
21. Van den Broeke, M. Strong surface melting preceded collapse of Antarctic Peninsula ice shelf. *Geophys. Res. Lett.* **32,** L12815 (2005).
22. Taylor, K. E., Stouffer, R. J. & Meehl, G. A. An overview of CMIP5 and the experiment design. *Bull. Am. Meteorol. Soc.* **93,** 485–498 (2012).
23. Abram, N. J. *et al.* Evolution of the Southern Annular Mode during the past millennium. *Nature Clim. Change* **4,** 564–569 (2014).
24. Van Angelen, J. H., van den Broeke, M. R., Wouters, B. & Lenaerts, J. T. M. Contemporary (1960–2012) evolution of the climate and surface mass balance of the Greenland ice sheet. *Surv. Geophys.* **35,** 1155–1174 (2013).
25. Holland, P. R. *et al.* Oceanic and atmospheric forcing of Larsen C ice-shelf thinning. *Cryosphere* **9,** 1005–1024 (2015).
26. Kuipers Munneke, P., Ligtenberg, S. R. M., van Den Broeke, M. R. & Vaughan, D. G. Firn air depletion as a precursor of Antarctic ice-shelf collapse. *J. Glaciol.* **60,** 205–214 (2014).

27. Pritchard, H. D. & Vaughan, D. G. Widespread acceleration of tidewater glaciers on the Antarctic Peninsula. *J. Geophys. Res.* **112,** F03S29 (2007).
28. Davies, B. J., Carrivick, J. L., Glasser, N. F., Hambrey, M. J. & Smellie, J. L. Variable glacier response to atmospheric warming, northern Antarctic Peninsula, 1988–2009. *Cryosphere* **6,** 1031–1048 (2012).
29. Braun, M., Humbert, A. & Moll, A. Changes of Wilkins ice shelf over the past 15 years and inferences on its stability. *Cryosphere* **3,** 41–56 (2009).
30. Holland, P. R., Jenkins, A. & Holland, D. M. The response of ice shelf basal melting to variations in ocean temperature. *J. Clim.* **21,** 2558–2572 (2008).

Acknowledgements

L.D.T. was supported by NASA Headquarters under the NASA Earth and Space Science Fellowship Program (grant NNX12AO01H) and the Doherty Postdoctoral Scholarship at the Woods Hole Oceanographic Institution. Funding for this research was additionally provided by the NASA Cryospheric Sciences Program (grant NNX10AP09G to S.B.D. and K.E.F.). M.R.v.d.B. and P.K.M. acknowledge support from the Netherlands Earth System Science Centre (NESSC) and the Polar Program of the Netherlands Organization of Scientific Research. The KNMI-RACMO2 simulations were supported by the Dutch Ministry of Infrastructure and the Environment. We acknowledge the World Climate Research Program's Working Group on Coupled Modelling, which is responsible for CMIP, and we thank the climate modelling groups (listed in Supplementary Table 3 of this paper) for producing and making available their model output. For CMIP the US Department of Energy's Program for Climate Model Diagnosis and Intercomparison provides coordinating support and led development of software infrastructure in partnership with the Global Organization for Earth System Science Portals.

Author contributions

L.D.T., K.E.F. and S.B.D. conceived the study. P.K.M., E.v.M. and M.R.v.d.B. performed RACMO2 simulations. L.D.T. led the data analysis and wrote the paper with contributions from K.E.F., S.B.D. and K.B.K. All authors contributed to interpretation of results and commented on the manuscript.

Additional information

Supplementary information is available in the online version of the paper. Reprints and permissions information is available online at www.nature.com/reprints. Correspondence and requests for materials should be addressed to L.D.T.

Competing financial interests

The authors declare no competing financial interests.

Methods

Melt–temperature sensitivity analysis. The relationship between ice shelf meltwater production and summer air temperature across a broad spectrum of climatic conditions was constrained using a combination of modelled and remotely sensed melt estimates. We used RACMO2.1 (ref. 31) forced at its lateral grid boundaries by both the ERA-Interim reanalysis[32] over 1980–2010 (ref. 7) and the EC-Earth2.3 GCM (ref. 33) under two future CMIP5 (ref. 22)/IPCC AR5-defined climate scenarios[34] (RCP4.5 and RCP8.5) over 2007–2100 as part of CORDEX (Coordinated Regional Climate Downscaling Experiment)[35]. RACMO2 has been extensively evaluated across Antarctica and found to reliably simulate both near-surface air temperature[36–39] and surface meltwater dynamics[7,8,17], among other critical variables of Antarctic climate. We supplemented modelled melt with independent satellite-based estimates of Antarctic surface meltwater production over the decade 2000–2009 (ref. 8) and combined these observations with modelled air temperatures from the ERA-Interim-forced RACMO2. The full melt–T_{2m} sensitivity analysis therefore included these observationally based meltwater fluxes and RACMO2-simulated melt using two different grid resolutions (27-km and 48-km) to account for methodological differences and spatial-resolution-induced biases. Further, to derive an idealized ice shelf melt–T_{2m} sensitivity relationship and minimize higher-frequency noise related to interannual surface energy balance variations, melt and T_{2m} data were averaged over decadal periods for specific ice shelves. Supplementary Table 1 details the ice shelves and data sets assessed in these analyses. A melt–temperature relationship derived using only ground and satellite observations confirms melt–temperature nonlinearity (Supplementary Fig. 6).

Melt modelling approaches. Two independent methods were employed to model the evolution of melt across Antarctica. First was the CORDEX-based forcing of RACMO2 by the well-suited EC-Earth2.3 GCM. To gain additional independent and computationally efficient estimates of melt trajectories, mean summer T_{2m} output from five low-bias CMIP5-based GCMs was analysed and converted to annual meltwater production using the established melt–T_{2m} sensitivity relationship (Fig. 1a). The following sections document the evaluation and selection of the CMIP5-based models used in these analyses.

CMIP5 model bias calculations and model selection. The ability of CMIP5-based GCMs to accurately reproduce Antarctic mean summer (DJF) near-surface (2-m) air temperature (T_{2m}) was examined to select the most ideal GCMs to simulate the evolution of Antarctic air temperature and derive meltwater production. As a reference T_{2m} data set to evaluate CMIP5 GCM performance, we used DJF-mean T_{2m} output from the higher-resolution (27-km) ERA-Interim forcing of RACMO2. Extensive existing validations of RACMO2 (refs 7,8,16,36–38), combined with its capability in overcoming limitations, including coarse spatial resolution and temperature biases known to exist in atmospheric reanalyses[39,40], present it as an ideal resource for GCM evaluation in Antarctica[41]. After first spatially interpolating GCM T_{2m} output to the (27-km) RACMO2 grid scale and MODIS-derived masking[42] of the simulations to include only Antarctic ice shelves, we calculated the Antarctic-wide spatially integrated ice shelf model bias, $\overline{\mathrm{Bias}_{\mathrm{GCM}}}$, using output from the respective Historical simulations of a total of 43 GCMs in the CMIP5 archive according to:

$$\overline{\mathrm{Bias}_{\mathrm{GCM}}} = \overline{T_{2\mathrm{m}_{\mathrm{GCM}}}} - \overline{T_{2\mathrm{m}_{\mathrm{RACMO\text{-}Era\text{-}Interim}}}} \quad (1)$$

where $\overline{T_{2\mathrm{m}_{\mathrm{GCM}}}}$ and $\overline{T_{2\mathrm{m}_{\mathrm{RACMO\text{-}Era\text{-}Interim}}}}$ are the mean DJF T_{2m} over a baseline period of 1980–2005 from each GCM and RACMO2 forced by ERA-Interim, respectively. A wide range of model biases were found, with the 43-model CMIP5 ensemble possessing a median positive DJF T_{2m} bias of 3.25 °C (Supplementary Fig. 7). Several models produced very low biases relative to the ERA-Interim-forced RACMO2, in particular those models using the NCAR Community Land Model version 4 (ref. 43; CLM4), shown in red in Supplementary Fig. 7. These five models are all unique in their full GCM set-ups by incorporating different configurations of atmospheric, ocean, or sea ice modules, but all share the common CLM4 land model. The five GCMs incorporating CLM4 well represent the mean climatology (5-model CLM4 ensemble mean bias = −0.60 °C). This low bias probably results from the sophistication of the CLM4 land/ice surface energy balance scheme relative to other GCMs. Notably, CLM4 calculates the multispectral albedo of snow surfaces, contains a multilayer snowpack, and simulates the evolution of snow grain size to prognostically determine albedo[43,44], all of which are important parameters to resolve for a realistic simulation of near-surface air temperature. Thus, because of their combination of low biases and relatively sophisticated land/ice surface schemes compared to other GCMs, those CMIP5 models incorporating CLM4 were specifically chosen in this study to simulate the evolution of Antarctic T_{2m}. We also note that biases with respect to the 48-km ERA-Interim forcing of RACMO2 are in close agreement with those presented above: 43-model CMIP5 ensemble median bias = 3.95 °C; 5-model CLM4 ensemble mean bias = 0.10 °C.

Bias assessment of GCM-forced RACMO2 simulations. In addition, we assessed the performance of two distinct GCM-forced RACMO2 simulations for their suitability in generating realistic twenty-first-century projections. As with the above GCM assessments, a low bias with respect to present-day conditions is necessary to interpret the model simulations as an evolution of contemporary melt conditions. Under CORDEX, RACMO2 was forced at its lateral boundaries by two GCMS: EC-Earth2.3 (as previously discussed) and HadGEM2-ES (ref. 45). Supplementary Table 2 shows the mean integrated Antarctic meltwater volume over 1980–2005 from two ERA-Interim forcings of RACMO2 and under the two GCM-forced Historical experiments. As in our GCM assessments described above, RACMO2 forced by ERA-Interim was used as a reference data set with which to assess model biases (Supplementary Table 2). This analysis revealed a very low bias (6.84 Gt yr^{-1}) in the RACMO2-EC-Earth Historical forcing during its temporal overlap with the primary reference data set, the reanalysis-driven RACMO2 at 27-km. Likewise, the bias between the RACMO2-EC-Earth Historical forcing and the 48-km ERA-Interim forcing approximates that between the two grid-resolution simulations of RACMO2 forced by the reanalysis. Such low biases produced by RACMO2 forced by EC-Earth support interpretation of its future melt simulations as a continuous evolution from present-day conditions. Conversely, large positive biases exist under the HadGEM2-ES forcing of RACMO2, with nearly 200% the Antarctic meltwater volume simulated over the recent past compared to the reanalysis forcings of RACMO2. As this study is primarily interested in assessing the potential future evolution of Antarctic melt with respect to present-day conditions, we exclusively considered the EC-Earth forcing of RACMO2.

GCM model bias adjustment and downscaling methods. To accurately model melt evolution from GCM-derived DJF T_{2m} output it is necessary to initialize projections at realistic air temperatures. For example, a GCM possessing a large negative T_{2m} bias would initially produce unrealistically low meltwater fluxes and, as a result, the twenty-first-century evolution of Antarctic melt would not be accurately represented. Thus, foremost critical is selection of GCMs with a low inherent bias, as described above. Despite having much lower overall biases than the multimodel CMIP5 median, each CLM4-incorporating GCM selected in this study still contains residual biases in their simulation of DJF T_{2m}. As such, following similar GCM bias correction and downscaling methods applied for melt modelling in Antarctica[46,47] and elsewhere[48], the DJF T_{2m} bias ($\overline{\mathrm{Bias}_{\mathrm{GCM}}}$ from equation (1)) calculated in each GCM grid cell was subtracted for each year of future simulation (t = 2007 to 2100) according to:

$$T_{2\mathrm{m}_{\mathrm{GCM,adjusted}}}(t) = T_{2\mathrm{m}_{\mathrm{GCM}}}(t) - \overline{\mathrm{Bias}_{\mathrm{GCM}}} \quad (2)$$

This process therefore preserved T_{2m} trends produced in each GCM while shifting the GCM T_{2m} output to the climatological DJF T_{2m} mean simulated by RACMO2 forced by ERA-Interim over the baseline period 1980–2005. This bias adjustment process was completed for each of the five selected GCMs (Supplementary Fig. 7) after first taking the mean of multiple ensemble runs for each model (if applicable; Supplementary Table 3) and then bilinearly interpolating the GCM output to the intermediate 48-km resolution used in future GCM-forced RACMO2 simulations. Because GCM output was spatially downscaled to the RACMO2 grid before the bias correction (that is, equation (2)), this method therefore also compensated for elevation-induced bias in the GCM. For example, if the GCM possessed a negative T_{2m} bias for a particular grid cell because the grid elevation is too high, the bias correction calculation (equation (2)) compensated for this by adding the temperature difference between the baseline Historical GCM simulation and the higher-spatial-resolution output from RACMO2 forced by ERA-Interim (from equation (1)). In accounting for elevation bias, this method therefore did not require application of subjective lapse rates, which are known to vary both spatially and temporally over glacier surfaces[49].

Deriving melt from GCM T_{2m} output. Following bias adjustment of future mean DJF T_{2m} simulations from the GCMs, the T_{2m} output of each model was converted to meltwater production, $\mathrm{Melt}_{\mathrm{GCM}}(t)$, in each year according to the exponential relationship obtained from the melt–T_{2m} sensitivity analysis (Fig. 1a):

$$\mathrm{Melt}_{\mathrm{GCM}}(t) = 1183 * \mathrm{e}^{(0.4557 * T_{2\mathrm{m}_{\mathrm{GCM,adjusted}}}(t))} \quad (3)$$

Thus, for each year of future simulation (t = 2007 to 2100) in each grid cell of the downscaled and bias-corrected GCM T_{2m} grid ($T_{2\mathrm{m}_{\mathrm{GCM,adjusted}}}(t)$), an annual GCM-derived meltwater flux (in mm w.e. yr^{-1}) was calculated. This conversion was applied to T_{2m} from each GCM and then ensemble statistics were calculated from the 5-model GCM Ensemble. Application of a low-melt threshold was necessary owing to the impossibility of deriving zero melt under equation (3). A value of 6 mm w.e. yr^{-1} (equivalent to −11.6 °C mean DJF T_{2m}) was chosen by minimizing the RMSE between the Antarctic-wide melt area simulated directly from RACMO2 forced by ERA-Interim and the melt area produced using T_{2m} from RACMO2 forced by ERA-Interim and equation (3). Finally, for consistency, both GCM and RACMO2 meltwater production grids were limited to a common land–ocean mask based on an updated version of the MODIS-derived coastline of Antarctica[42].

Code and data availability. CMIP5 (ref. 22) model output and RACMO2 experiments under CORDEX (ref. 35) are available from the Earth System Grid Federation: http://pcmdi9.llnl.gov. ERA-Interim-forced RACMO2 simulations at 27-km grid resolution are available on request at http://www.projects.science.uu.nl/iceclim/models/data.php. QuikSCAT melt estimates[8] are available on request from L.D.T. James Ross Island ice core melt data[11] are available from ftp://ftp.ncdc.noaa.gov/pub/data/paleo/icecore/antarctica/james-ross-island/james-ross-island2013.txt. *In situ* temperature observations are available from the SCAR READER project[19]: https://legacy.bas.ac.uk/met/READER/data.html. ERA-Interim reanalysis[32] data are available from http://apps.ecmwf.int/datasets/data/interim-full-moda. Code generated to implement bias assessment and conversion of GCM T_{2m} to meltwater fluxes (equations (1)–(3)) available on request to L.D.T.

References

31. Van Meijgaard, E. *et al. The KNMI Regional Atmospheric Climate Model RACMO, Version 2.1.* Technical Report (KNMI, 2008).
32. Dee, D. P. *et al.* The ERA-Interim reanalysis: Configuration and performance of the data assimilation system. *Q. J. R. Meteorol. Soc.* **137,** 553–597 (2011).
33. Hazeleger, W. *et al.* EC-Earth V2.2: Description and validation of a new seamless Earth system prediction model. *Clim. Dynam.* **39,** 2611–2629 (2012).
34. Van Vuuren, D. P. *et al.* The representative concentration pathways: An overview. *Climatic Change* **109,** 5–31 (2011).
35. Giorgi, F., Jones, C. & Asrar, G. R. Addressing climate information needs at the regional level: The CORDEX framework. *Bull. World Meteorol. Org.* **58,** 175–183 (2009).
36. Van den Broeke, M. Depth and density of the Antarctic firn layer. *Arct. Antarct. Alp. Res.* **40,** 432–438 (2008).
37. Van Lipzig, N. P. M., Marshall, G. J., Orr, A. & King, J. C. The relationship between the Southern Hemisphere Annular Mode and Antarctic Peninsula Summer Temperatures: Analysis of a high-resolution model climatology. *J. Clim.* **21,** 1649–1668 (2008).
38. Lenaerts, J. T. M. *et al.* Modeling drifting snow in Antarctica with a regional climate model: 1. Methods and model evaluation. *J. Geophys. Res.* **117,** D05108 (2012).
39. Reijmer, C. H., van Meijgaard, E. & van den Broeke, M. R. Evaluation of temperature and wind over Antarctica in a regional atmospheric climate model using 1 year of automatic weather station data and upper air observations. *J. Geophys. Res.* **110,** D04103 (2005).
40. Van de Berg, W. J., van den Broeke, M. R., Reijmer, C. H. & van Meijgaard, E. Characteristics of the Antarctic surface mass balance, 1958–2002, using a regional atmospheric climate model. *Ann. Glaciol.* **41,** 97–104 (2005).
41. Maris, M. N. A., de Boer, B. & Oerlemans, J. A climate model intercomparison for the Antarctic region: Present and past. *Clim. Past* **8,** 803–814 (2012).
42. Haran, T., Bohlander, J., Scambos, T., Painter, T. & Fahnestock, M. *MODIS Mosaic of Antarctica (MOA) Image Map* (National Snow and Ice Data Center, 2005).
43. Lawrence, D. M. *et al.* Parameterization improvements and functional and structural advances in Version 4 of the Community Land Model. *J. Adv. Model. Earth Syst.* **3,** M03001 (2011).
44. Oleson, K. *et al. Technical Description of Version 4.0 of the Community Land Model (CLM) 257* Report No. NCAR/TN-4781STR (NCAR, 2010).
45. Jones, C. D. *et al.* The HadGEM2-ES implementation of CMIP5 centennial simulations. *Geosci. Model Dev.* **4,** 543–570 (2011).
46. Fyke, J. G., Carter, L., Mackintosh, A., Weaver, A. J. & Meissner, K. J. Surface melting over ice shelves and ice sheets as assessed from modeled surface air temperatures. *J. Clim.* **23,** 1929–1936 (2010).
47. Radic, V. & Hock, R. Regionally differentiated contribution of mountain glaciers and ice caps to future sea-level rise. *Nature Geosci.* **4,** 91–94 (2011).
48. Radić, V. & Hock, R. Modeling future glacier mass balance and volume changes using ERA-40 reanalysis and climate models: A sensitivity study at Storglaciären, Sweden. *J. Geophys. Res.* **111,** F03003 (2006).
49. Gardner, A. S. *et al.* Near-surface temperature lapse rates over Arctic glaciers and their implications for temperature downscaling. *J. Clim.* **22,** 4281–4298 (2009).

nature geoscience

SUPPLEMENTARY INFORMATION

DOI: 10.1038/NGEO2563

Divergent trajectories of Antarctic surface melt under two twenty-first-century climate scenarios

Luke D. Trusel[1,2*], Karen E. Frey[2], Sarah B. Das[1], Kristopher B. Karnauskas[1], Peter Kuipers Munneke[3,4], Erik van Meijgaard[5], Michiel R. van den Broeke[3]

1 Department of Geology and Geophysics, Woods Hole Oceanographic Institution, Woods Hole, MA, 02543, USA
2 Graduate School of Geography, Clark University, Worcester, MA, 01610, USA
3 Institute for Marine and Atmospheric Research, Utrecht University, 3508 TA Utrecht, Netherlands
4 Swansea University, Department of Geography, Swansea, SA2 8PP, United Kingdom
5 Royal Netherlands Meteorological Institute, 3730 AE De Bilt, Netherlands
* Email: ltrusel@whoi.edu

Contains:

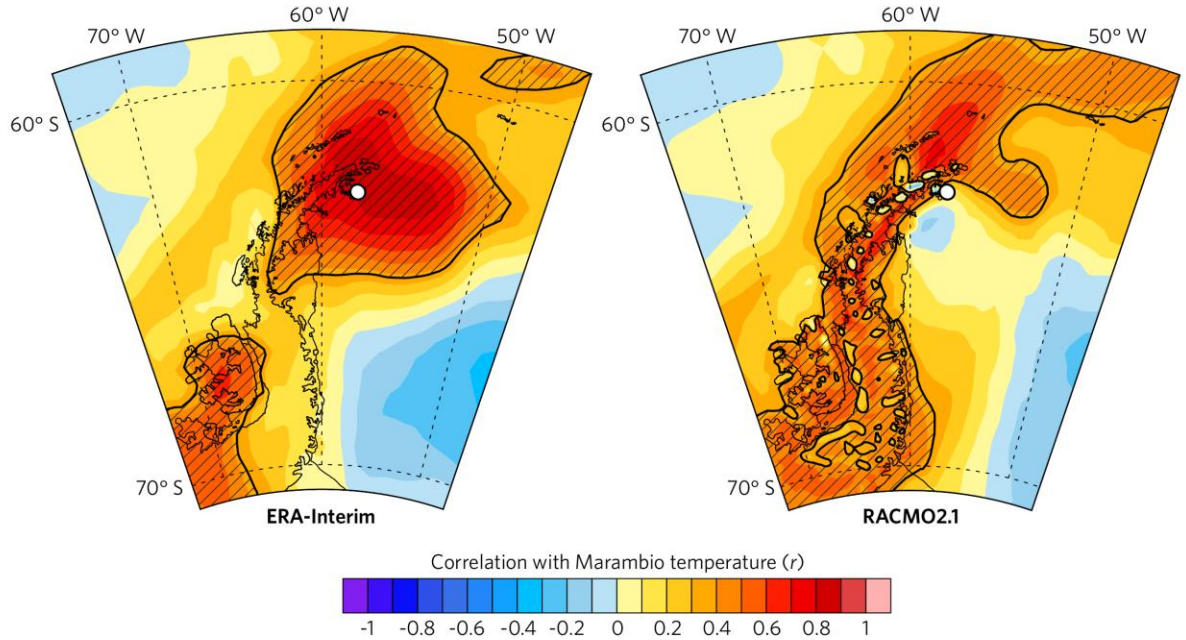

Supplementary Figure 1.
Spatial correlation coefficients (r) between observed DJF temperatures at Base Marambio[1] (location indicated by white dots) and DJF T_{2m} from ERA-Interim and RACMO over 1981–2009 (the time period of overlap with continuous observations). Areas of significant ($p \leq 0.05$) correlation indicated by hatching. Observed temperatures at Marambio broadly correlate with reanalyzed and modeled temperatures, particularly across the northeast Antarctic Peninsula and its ice shelves. As such, observed interannual summer temperature variability at Marambio can be interpreted as representative of broader Antarctic Peninsula conditions.

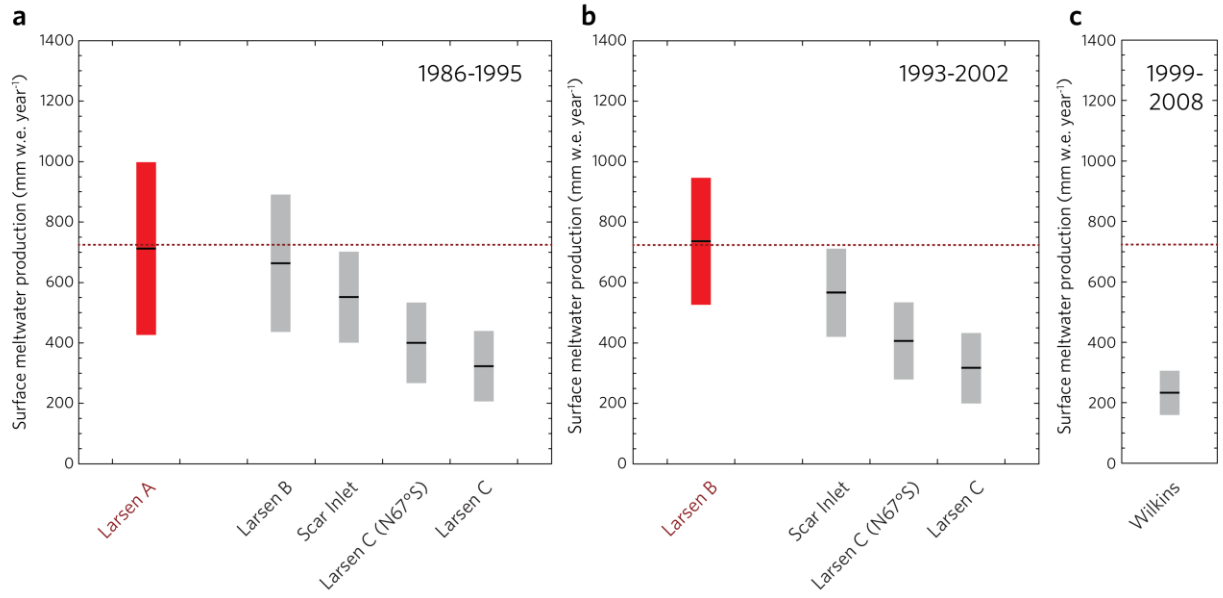

Supplementary Figure 2.
Mean melting conditions (± 1 temporal standard deviation) on Antarctic Peninsula ice shelves over the decades preceding the abrupt collapses of Larsen A (**a**, 1986–1995) and Larsen B (**b**, 1993–2002), and the more gradual breakup of Wilkins (**c,** 1999–2008). Melt data were averaged from two simulations of RACMO2 forced by ERA-Interim (27 and 48-km resolution), with the exception of Larsen A which was only resolved at 27-km resolution (Supplementary Table 1). Horizontal red dotted lines show the average pre-collapse melt of Larsen A and B (725 mm w.e. year^{-1}; as in Fig. 3b). Mean melt levels on northeast Antarctic Peninsula ice shelves that have remained intact (i.e., Scar Inlet, the high melt region of Larsen C north of 67°S, and Larsen C as a whole), experienced significantly ($p \leq 0.05$; two-tailed *t*-test) less melt than Larsen A and Larsen B. Whereas melt on the portion of Larsen B that collapsed in 2002 was not significantly different than Larsen A over 1986–1995 (**a**), its collapse followed rapid regional warming and coincided with extreme melt in 2002 (e.g., Fig. 2a). These results further demonstrate the linkage between locally high ice shelf melting and collapse events, while also supporting previous studies that have identified strong surface melt and hydrofracture as a leading mechanism in the abrupt collapses of Larsen A and B[2–4]. As an additional test of pre-breakup melt levels, we examined RACMO2-simulated melt on Wilkins Ice Shelf of the southwestern Antarctic Peninsula (**c**). This ice shelf has recently experienced more gradual retreat relative to Larsen A and B, with several breakup events occurring in summer, autumn, and winter of 2008 (for example, ref. 5). We find that in the decade preceding the 2008 Wilkins retreat, melt was significantly lower than that occurring on Larsen A and B before their abrupt collapses. This result supports work suggesting that surface melt played a more limited role in the breakup of Wilkins[6,7]. Nonetheless, others suggest the May 2008 breakup event may still have been in part related to surface melt-induced hydrofracture[5], underscoring the underlying complexity of ice shelf stability and response to external forcing.

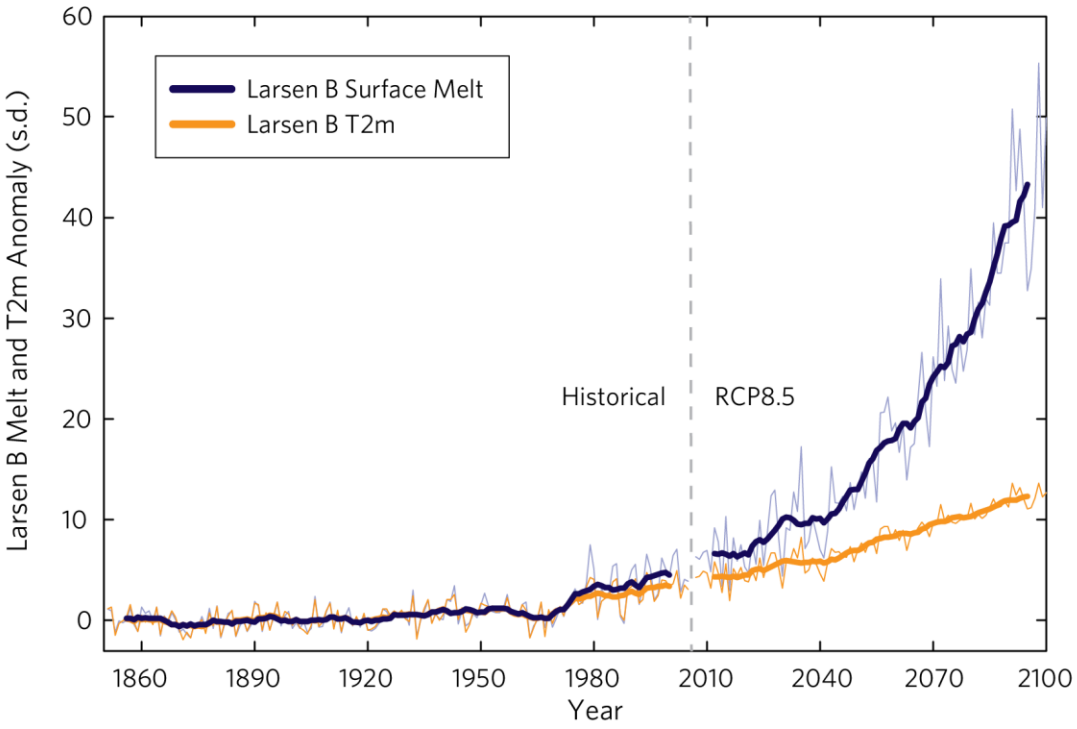

Supplementary Figure 3.
Anomalies in melt and temperature (with respect to 1851–1900) across Larsen B ice shelf. Anomalies from the GCM Ensemble Historical simulations (1851–2005) are shown as in Fig. 2c, whereas anomalies in the RCP8.5 scenario (2007–2100) are derived from the remaining portion of Larsen B ice shelf in Scar Inlet. Anomalies in melt far exceed anomalies in temperature owing to melt-temperature nonlinearity (see Fig. 1a).

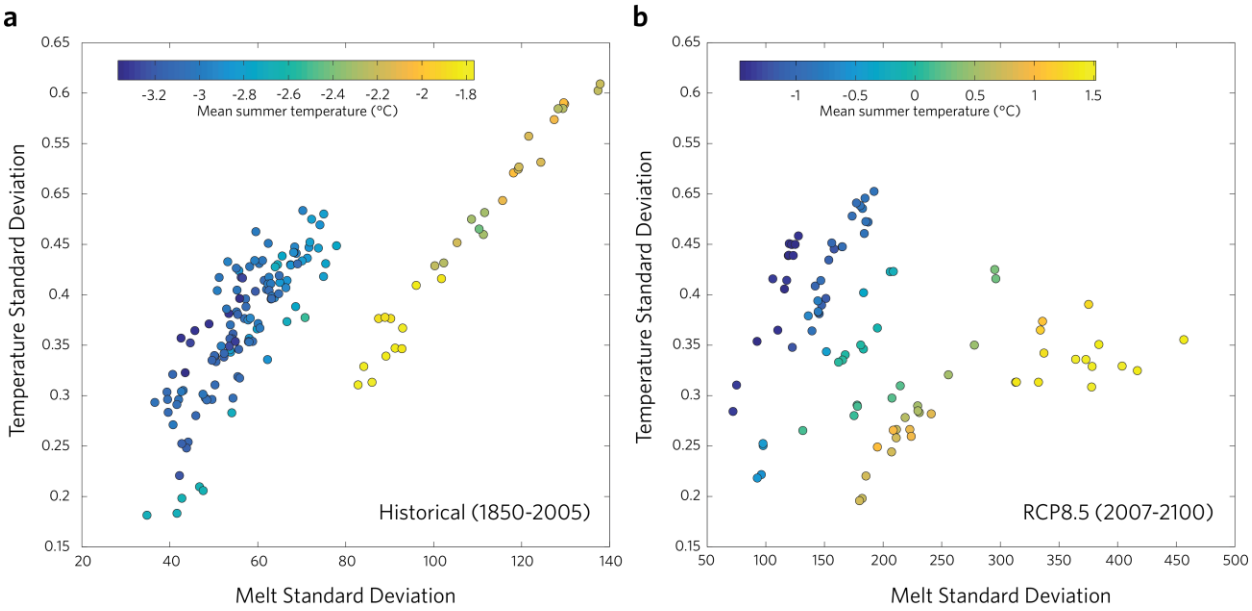

Supplementary Figure 4.
Plots of the 11-year moving temporal standard deviation of temperature and melt on Larsen B from Historical simulations (**a**) and RCP8.5 (**b**). Points are colored by mean summer temperature. (**a**) Abrupt warming occurring circa 1970 (Fig. 2b) resulted in a shift to higher interannual melt variability owing to the nonlinearity of melt in response to changing summer air temperature (Fig. 1a). (**b**) More gradual shifts toward higher interannual melt variability are simulated under a progressive RCP8.5 warming. Note unique x-axes.

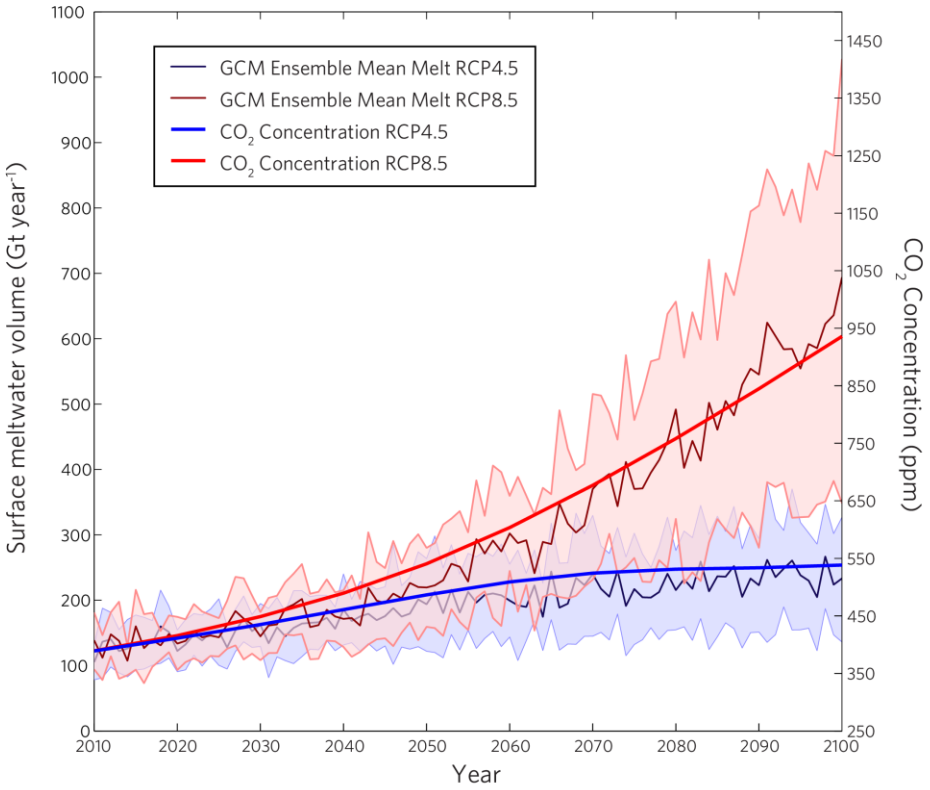

Supplementary Figure 5.
A clear connection exists between the projected Antarctic meltwater volume and atmospheric CO_2 concentrations under RCP4.5 and RCP8.5 (CO_2 time series from ref. 8). The future volume of meltwater produced at the Antarctic ice sheet surface is a function of future changes in radiative forcing, in which atmospheric CO_2 concentrations play an integral role.

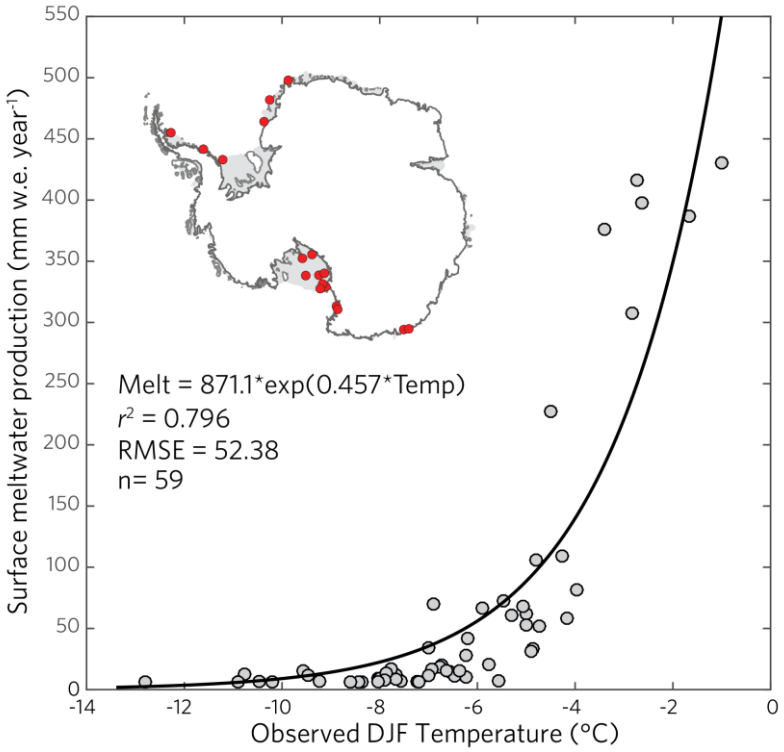

Supplementary Figure 6.
An observationally constrained melt-temperature relationship using satellite-derived surface meltwater production from QuikSCAT[9] and mean summer (DJF) air temperatures at 18 AWS and research station locations in the SCAR READER database[1] (red points on map). We examined all locations over ice with complete DJF observations during at least one year of the QuikSCAT record (1999–2000 to 2000–2009) and within a QuikSCAT grid cell detected as melting. Annual meltwater production estimated from QuikSCAT was taken from the corresponding year and grid cell containing each air temperature observation. Despite challenges inherent to this comparison including temporal mismatch between observation methods and the coarse satellite spatial resolution relative to the point scale[10], a strong nonlinear melt-temperature relationship is evident and well characterized by an exponential regression model (black line). The derived exponential relationship is strong, although data paucity at intermediate and high melt-temperature levels limit its predictive ability. This relationship is nevertheless in close agreement with our main (and independent) melt-T_{2m} sensitivity analysis that is constrained largely by coupled-climate snowpack modeling (Fig. 1a), and thereby provides additional, empirical support for melt-T_{2m} nonlinearity across Antarctica.

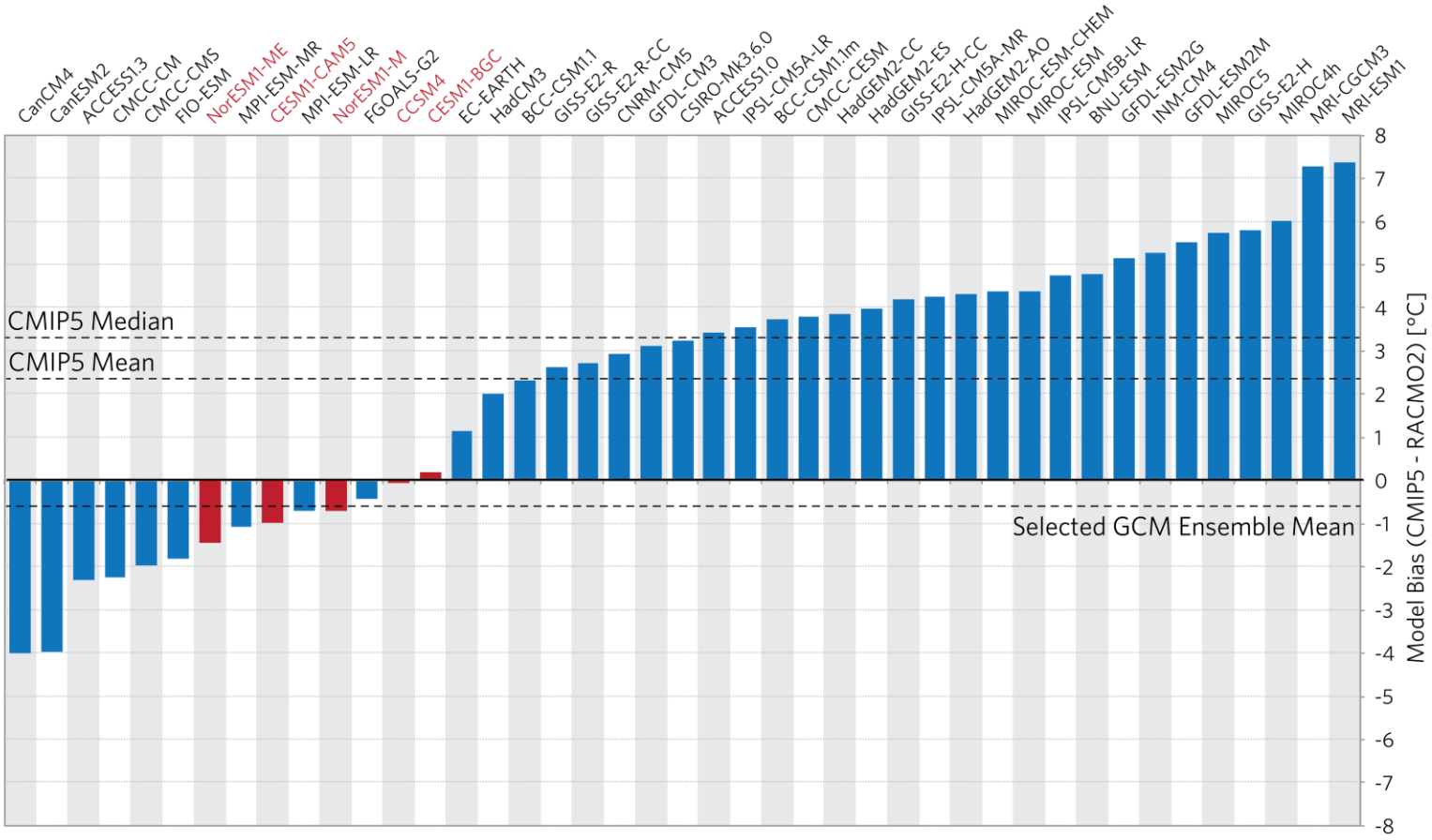

Supplementary Figure 7.
Absolute DJF-mean T_{2m} bias over all Antarctic ice shelves for 43 CMIP5-based[11] GCMs relative to ERA-Interim-forced RACMO2 at 27-km. Models selected for their Antarctic T_{2m} projections are indicated in red (see Supplementary Table 3), as are the mean DJF T_{2m} biases of these selected models and mean and median biases of the broader CMIP5 multimodel ensemble.

	Ice Shelf	**QuikSCAT** 2000-2009	**RACMO2** (27-km) ERA-Interim 1980-2009	**RACMO2** (48-km) ERA-Interim 1980-2009	**RACMO2** EC-Earth RCP4.5 2010-2099	**RACMO2** EC-Earth RCP8.5 2010-2099
AP	Bach	1 (225)	3 (6)	3 (2)	9 (2)	9 (2)
AP	George VI	1 (1186)	3 (31)	3 (9)	9 (9)	9 (9)
AP	Larsen A	No data	1 (5)	No data	No data	No data
AP	Larsen B	No data	2 (6)	2 (2)	No data	No data
AP	Larsen C	1 (2490)	3 (59)	3 (22)	9 (22)	9 (22)
AP	Larsen D	1 (1193)	3 (31)	3 (10)	9 (10)	9 (10)
AP	Scar Inlet	1 (141)	3 (3)	3 (1)	9 (1)	9 (1)
AP	Stange	1 (586)	3 (18)	3 (5)	9 (5)	9 (5)
AP	Wilkins	1 (698)	3 (17)	3 (6)	9 (6)	9 (6)
WA	Abbot	1 (1625)	3 (42)	3 (16)	9 (16)	9 (16)
WA	Cosgrove	1 (150)	3 (4)	3 (2)	9 (2)	9 (2)
WA	Crosson	1 (122)	3 (3)	3 (2)	9 (2)	9 (2)
WA	Dotson	1 (236)	3 (5)	3 (2)	9 (2)	9 (2)
WA	Getz	1 (1686)	3 (49)	3 (14)	9 (14)	9 (14)
WA	Nickerson	1 (362)	3 (7)	3 (2)	9 (2)	9 (2)
WA	Pine Island	1 (304)	3 (7)	3 (2)	9 (2)	9 (2)
WA	Ross	1 (24307)	3 (652)	3 (215)	9 (215)	9 (215)
WA	Sulzberger	1 (680)	3 (19)	3 (6)	9 (6)	9 (6)
WA	Thwaites	1 (219)	3 (6)	3 (2)	9 (2)	9 (2)
WA	Venable	1 (164)	3 (3)	3 (2)	9 (2)	9 (2)
WL	Amery	1 (2876)	3 (71)	3 (29)	9 (29)	9 (29)
WL	Conger	1 (125)	3 (3)	3 (2)	9 (2)	9 (2)
WL	Cook	1 (214)	3 (5)	3 (3)	9 (3)	9 (3)
WL	Dibble	1 (79)	3 (2)	3 (1)	9 (1)	9 (1)
WL	Holmes	1 (94)	3 (3)	3 (1)	9 (1)	9 (1)
WL	Mertz	1 (295)	3 (9)	3 (2)	9 (2)	9 (2)
WL	Moscow	1 (250)	3 (7)	3 (1)	9 (1)	9 (1)
WL	Publications	1 (87)	3 (3)	3 (1)	9 (1)	9 (1)
WL	Rennick	1 (124)	3 (2)	3 (1)	9 (1)	9 (1)
WL	Shackleton	1 (1729)	3 (41)	3 (15)	9 (15)	9 (15)
WL	Totten	1 (401)	3 (12)	3 (3)	9 (3)	9 (3)
WL	West	1 (866)	3 (21)	3 (8)	9 (8)	9 (8)
DML	Atka	1 (99)	3 (2)	3 (1)	9 (1)	9 (1)
DML	Baudouin	1 (1664)	3 (44)	3 (14)	9 (14)	9 (14)
DML	Borchgrevink	1 (876)	3 (23)	3 (9)	9 (9)	9 (9)
DML	Brunt	1 (1683)	3 (44)	3 (13)	9 (13)	9 (13)
DML	Unnamed (23°E)	1 (190)	3 (5)	3 (2)	9 (2)	9 (2)
DML	Ekstrom	1 (356)	3 (9)	3 (3)	9 (3)	9 (3)
DML	Filchner	1 (5108)	3 (135)	3 (46)	9 (46)	9 (46)
DML	Fimbul	1 (2057)	3 (56)	3 (19)	9 (19)	9 (19)
DML	Jelbart	1 (561)	3 (15)	3 (6)	9 (6)	9 (6)
DML	Lazarev	1 (434)	3 (12)	3 (4)	9 (4)	9 (4)
DML	Nivl	1 (379)	3 (12)	3 (5)	9 (5)	9 (5)
DML	Prince Harald	1 (269)	3 (7)	3 (3)	9 (3)	9 (3)

DML	Quar	1 (112)	3 (2)	3 (1)	9 (1)	9 (1)
DML	Riiser-Larsen	1 (2293)	3 (63)	3 (26)	9 (26)	9 (26)
DML	Ronne	1 (16445)	3 (435)	3 (145)	9 (145)	9 (145)
DML	Vigrid	1 (118)	3 (2)	3 (1)	9 (1)	9 (1)

Supplementary Table 1.
Listing of observed and modeled data used to establish the melt-T_{2m} sensitivity and calibration curve show in Fig. 1a. Values of each cell indicate the number of data points (i.e., decadal periods) from each method for particular ice shelves and floating outlet glacier termini in Fig 1a. Values in parentheses indicate number of discrete grid cells available in each method for each ice shelf after masking with an updated version of the MODIS outline of Antarctica[12]. For the melt-T_{2m} calibration (Fig. 1a), T_{2m} data coinciding with QuikSCAT melt observations[9] were taken from RACMO2 forced by ERA-Interim at 27-km grid resolution. All melt and T_{2m} data were averaged spatially across ice shelf grid cells and decadally beginning in 2000–2009 for consistency between reanalysis-forced RACMO2 simulations and QuikSCAT observations. An exception exists for Larsen A and B (in Fig. 1a, Fig. 1b, and Supplementary Fig. 2), for which data were averaged over available decades ending in the years associated with their collapses (i.e., 1986–1995 for Larsen A, 1993–2002 for Larsen B). Ice shelves are organized in this table by region indicated in first column and shown in Fig. 4b (AP: Antarctic Peninsula; WA: West Antarctica; WL: Wilkes Land; DML: Dronning Maud Land). Note that after spatial downscaling and bias correction, the number of grid cells used in future projections from the GCM Ensemble (i.e., Figs. 3b, 4a) are identical to that as RACMO2 at 48-km.

	RACMO2-ERA-Interim 27-km	**RACMO2-ERA-Interim 48-km**	**RACMO2-EC-Earth (Historical)**	**RACMO2-HadGEM2-ES (Historical)**
Mean Antarctic meltwater volume (1980–2005) (Gt $year^{-1}$)	105.59	83.43	112.43	199.09
Bias (w.r.t. RACMO2-ERA-Interim 27-km) (Gt $year^{-1}$)	-	-22.16	6.84	93.51
Bias (w.r.t. RACMO2-ERA-Interim 48-km) (Gt $year^{-1}$)	22.16	-	29.00	115.67

Supplementary Table 2.
Biases in the Antarctic-wide meltwater volume simulated between RACMO2 forced by ERA-Interim at two grid resolutions and two GCMs under their CMIP5 Historical experiments. RACMO2 forced by EC-Earth produces very similar results to the ERA-Interim forcings, whereas RACMO2 forced by HadGEM2-ES shows large positive melt biases.

Model	Spatial Resolution	Driving Dataset	Timespans utilized (CMIP5 Experiment)	Ensemble members
RACMO2	27-km	ERA-Interim Reanalysis (ref. 13)	1980-2010	1
RACMO2	48-km	ERA-Interim Reanalysis (ref. 13)	1980-2012	1
RACMO2	48-km	EC-Earth2.3 (r1i1p1) (ref. 14)	2007-2100 (RCP4.5, RCP8.5)	1 (all experiments)
CCSM4 (ref. 15)	1.25° longitude, 0.94° latitude	N/A	1851-2005 (historicalNat) 1980-2005 (Historical) 2007-2100 (RCP4.5, RCP8.5)	4 (historicalNat) 6 (Historical, RCP4.5, RCP8.5)
CESM1(BGC) (ref. 16)	1.25° longitude, 0.94° latitude	N/A	1980-2005 (Historical) 2007-2100 (RCP4.5, RCP8.5)	1 (all experiments)
CESM1(CAM5) (ref. 17)	1.25° longitude, 0.94° latitude	N/A	1851-2005 (historicalNat) 1980-2005 (Historical) 2007-2100 (RCP4.5, RCP8.5)	3 (all experiments)
NorESM1-M (ref. 18)	2.5° longitude, 1.895° latitude	N/A	1851-2005 (historicalNat) 1980-2005 (Historical) 2007-2100 (RCP4.5, RCP8.5)	3 (Historical) 1 (historicalNat, RCP4.5, RCP8.5)
NorESM1-ME (ref. 18)	2.5° longitude, 1.895° latitude	N/A	1980-2005 (Historical) 2007-2100 (RCP4.5, RCP8.5)	1 (all experiments)

Supplementary Table 3.
Regional and global climate model configurations used in this study. Where multiple ensemble members were available, the ensemble mean was calculated. Whereas Historical experiments (i.e., including all transient forcing agents) were available from the five GCMs, historicalNat (i.e., including only natural forcing agents) were only available from three.

Supplementary References

1. Turner, J. *et al.* The SCAR READER Project: Toward a High-Quality Database of Mean Antarctic Meteorological Observations. *J. Climate* **17,** 2890–2898 (2004).
2. Vaughan, D. G. & Doake, C. S. M. Recent atmospheric warming and retreat of ice shelves on the Antarctic Peninsula. *Nature* **379,** 328–331 (1996).
3. Scambos, T. A., Hulbe, C., Fahnestock, M. & Bohlander, J. The link between climate warming and break-up of ice shelves in the Antarctic Peninsula. *J. Glaciol.* **46,** 516–530 (2000).
4. Scambos, T., Hulbe, C. & Fahnestock, M. in *Antarctic Research Series* (eds. Domack, E. et al.) **79,** 79–92 (American Geophysical Union, 2003).
5. Scambos, T. *et al.* Ice shelf disintegration by plate bending and hydro-fracture: Satellite observations and model results of the 2008 Wilkins ice shelf break-ups. *Earth Planet. Sc. Lett.* **280,** 51–60 (2009).
6. Braun, M. & Humbert, A. Recent Retreat of Wilkins Ice Shelf Reveals New Insights in Ice Shelf Breakup Mechanisms. *IEEE Geosci. Remote S.* **6,** 263–267 (2009).
7. Braun, M., Humbert, A. & Moll, A. Changes of Wilkins Ice Shelf over the past 15 years and inferences on its stability. *Cryosphere* **3,** 41–56 (2009).
8. Van Vuuren, D. P. *et al.* The representative concentration pathways: an overview. *Climatic Change* **109,** 5–31 (2011).
9. Trusel, L. D., Frey, K. E., Das, S. B., Kuipers Munneke, P. & van den Broeke, M. R. Satellite-based estimates of Antarctic surface meltwater fluxes. *Geophys. Res. Lett.* **40,** 6148–6153 (2013).
10. Trusel, L. D., Frey, K. E. & Das, S. B. Antarctic surface melting dynamics: Enhanced perspectives from radar scatterometer data. *J. Geophys. Res.* **117,** F02023 (2012).
11. Taylor, K. E., Stouffer, R. J. & Meehl, G. A. An Overview of CMIP5 and the Experiment Design. *Bull. Amer. Meteorol. Soc.* **93,** 485–498 (2012).
12. Haran, T., Bohlander, J., Scambos, T., Painter, T. & Fahnestock, M. *MODIS Mosaic of Antarctica (MOA) Image Map* (National Snow and Ice Data Center, Boulder, 2005).
13. Dee, D. P. *et al.* The ERA-Interim reanalysis: configuration and performance of the data assimilation system. *Q. J. R. Meteorol. Soc.* **137,** 553–597 (2011).
14. Hazeleger, W. *et al.* EC-Earth V2.2: description and validation of a new seamless earth system prediction model. *Clim. Dyn.* **39,** 2611–2629 (2012).
15. Gent, P. R. *et al.* The Community Climate System Model Version 4. *J. Climate* **24,** 4973–4991 (2011).
16. Long, M. C., Lindsay, K., Peacock, S., Moore, J. K. & Doney, S. C. Twentieth-Century Oceanic Carbon Uptake and Storage in CESM1(BGC)*. *J. Climate* **26,** 6775–6800 (2013).
17. Meehl, G. A. *et al.* Climate Change Projections in CESM1(CAM5) Compared to CCSM4. *J. Climate* **26,** 6287–6308 (2013).
18. Bentsen, M. *et al.* The Norwegian Earth System Model, NorESM1-M – Part 1: Description and basic evaluation of the physical climate. *Geosci. Model Dev.* **6,** 687–720 (2013).